Materials Today Advances 6 (2020) 100066

Contents lists available at ScienceDirect

Materials Today Advances

journal homepage: www.journals.elsevier.com/materials-today-advances/

Biodegradable zinc-containing mesoporous silica nanoparticles for cancer therapy

S. Chen [a], S.L. Greasley [a], Z.Y. Ong [a], P. Naruphontjirakul [a, e], S.J. Page [b], J.V. Hanna [b], A.N. Redpath [c], O. Tsigkou [d], S. Rankin [c], M.P. Ryan [a], A.E. Porter [a], J.R. Jones [a, *]

[a] Department of Materials, Imperial College London, South Kensington Campus, SW7 2AZ, UK
[b] Department of Physics, University of Warwick, Gibbet Hill Road, Coventry CV4 7AL, UK
[c] National Heart and Lung Institute, Imperial College London, South Kensington Campus, SW7 2AZ, UK
[d] Department of Materials, University of Manchester, Manchester, M13 9PL, UK

ARTICLE INFO

Article history:
Received 31 December 2019
Accepted 6 March 2020
Available online xxx

Keywords:
Triple-negative breast cancer
Zinc
Bioactive nanoparticle
Cellular uptake

ABSTRACT

Triple-negative breast cancers are extremely aggressive with limited treatment options because of the reduced response of the cancerous cells to hormonal therapy. Here, monodispersed zinc-containing mesoporous silica nanoparticles (MSNPs-Zn) were produced as a tuneable biodegradable platform for delivery of therapeutic zinc ions into cells. We demonstrate that the nanoparticles were internalized by cells, and a therapeutic dose window was identified in which the MSNPs-Zn were toxic to breast cancer cells but not to healthy epithelial (MCF-10a) cells or to murine macrophages. A significant reduction in the viability of triple negative MDA-MB-231 and MCF-7 (ER+) breast cancer cells was seen following 24 h exposure to MSNPs-Zn. The more aggressive MDA-MB-231 cells, with higher metastatic potential, were more sensitive to MSNPs-Zn than the MCF-7 cells. MSNPs-Zn underwent biodegradation inside the cells, becoming hollow structures, as imaged by high-resolution transmission electron microscopy. The mesoporous silica nanoparticles provide a biodegradable vehicle for therapeutic ion release inside cells.

1. Introduction

Triple-negative breast cancers (TNBCs) are an extremely aggressive form of breast cancer with a high risk of distant metastasis. Treatment options for TNBCs are limited because these cells do not respond to hormonal therapy [1]. TNBC patients often need to be treated with systemic chemotherapy, which has low tumor selectivity, as the chemotherapeutics diffuse and distribute non-specifically throughout the body after drug administration, resulting in unwanted side-effects. Multidrug resistance, resulting from decreased cell uptake and increased efflux of drugs, has also become a challenge to successful TNBC cancer treatment. Therefore, development of novel therapies for TNBCs is urgently needed.

Nanomaterials hold great promise as new tools for treatment of cancers, providing platforms that deliver theranostic (combined therapeutic and diagnostic) functionality directly to tumors. Mesoporous silica nanoparticles (MSNPs) have been investigated as one of the most promising drug delivery systems for cancer treatment because of the excellent biocompatibility of silica and their porous structure, which is ideal for drug loading [2–5]. The need to prevent premature drug leakage from the pores in the bloodstream and ensuring they reach the correct cells by targeting is a great challenge [6]. MSNPs modified with a lipid bilayer coating and targeting peptides have been assembled as synthetic 'protocells' that can deliver a combination of therapeutic agents selectively to target cells [7,8]. *In vitro* success saw protocells kill drug-resistant human hepatocellular carcinoma cells [7] and leukemia cell lines *ex ovo* in a chick chorioallantoic membrane model [8]. A complementary, simpler, more universal, lower risk system would be desirable to reduce time to approval for clinical use, especially as only 0.9% of nanoparticles reach their intended target, even when using active targeting [9].

A concern over the use of silica as a delivery vehicle has been that it may remain in the body long term. However, the physicochemical properties of silica can be altered at the atomic level by introducing modifier cations the in Si–O network. For example, bioactive glass, which is amorphous silica containing Ca^{2+}, Na^{+}, and phosphate, used as a clinical synthetic bone graft for over 20 years, has been

* Corresponding author.
E-mail address: julian.r.jones@imperial.ac.uk (J.R. Jones).
[e] Now at: Biological Engineering Program, Faculty of Engineering, King Mongkut's University of Technology Thonburi, Bangkok 10140, Thailand.

https://doi.org/10.1016/j.mtadv.2020.100066

shown to be an excellent biodegradable biomaterial [10–13]. Inspired by bioactive glasses, cation containing silica particles have been developed to provide therapeutic functions, depending on the choice of cation [14–21]. However, because of the challenge of incorporating the therapeutic cations, while maintaining monodispersity, only a very limited number of studies have been reported on this type of nanoparticle [21,22]. Mitchell et al. developed iron-doped silica nanoshells as magnetic resonance imaging (MRI) contrast agents, which were grown on the surface of polystyrene sphere templates, which were removed later by calcination [15]. Ca-containing MSNPs were produced by adding $Ca(NO_3)_2$ and triethyl phosphate into the sol-gel reaction, using cetyltrimethylammonium bromide (CTAB) as a template, and an *in vitro* study demonstrated that Ca incorporation accelerated the degradation rate of MSNPs [23]. Recently, hollow manganese-doped mesoporous silica NPs were also developed as biodegradable drug delivery systems with T_1 MRI contrast enhancement properties, Mn being selected for its low toxicity and good T_1 relaxivity, by treating presynthesized MSNPs with $MnSO_4$ under hydrothermal conditions [17]. These studies have shown the potential of silica-based glass MSNPs for delivering chemotherapeutic drugs to tumors; however, there have been no studies which have exploited the therapeutic properties of specific cations themselves to treat cancer. An obstacle to the development of these materials is to overcome the synthesis challenge of preserving the mesoporous structure of MSNPs and to control the cation incorporation while simultaneously tuning the biodegradability and ion release rates of the nanoparticle silica platforms. The mechanisms by which ion-doped silica nanoparticles are degraded within cells remain largely unknown [24].

Here, we report on monodispersed zinc-containing silica-based mesoporous bioactive glass nanoparticles (MSNPs-Zn) as a tuneable biodegradable platform for delivering of therapeutic zinc ions into cells. Zinc is involved in growth and normal development and participates in many physiological processes. Zinc ions have been shown to preferentially kill bacteria and to have potential as an anticancer treatment in the form of zinc oxide [25,26]. ZnO nanowires showed selective toxicity with breast cancer cells *in vitro* [27]. A dose window exists within which the zinc oxide NPs caused a significant reduction in the cell viability of cancer cells while the healthy cells remain protected [25,26]. The problem is that ZnO undergoes biodegradation rapidly, so would dissolve soon after being introduced into the blood stream, not reaching its target. The biodegradable mesoporous system developed here offers greater flexibility to incorporate additional therapeutic functionality into the platform for more effective *in vivo* performance. As the Zn^{2+} ions are within a silica matrix, delaying zinc on release is delayed compared with the ZnO nanowires. The control over particle size, pore size, and zinc content is highly beneficial. SiO_2–CaO–ZnO nanoparticles were recently produced, but the focus was on the effect of zinc addition on apatite formation with a view to bone repair [28].

Here, a new biodegradable monodispersed mesoporous SiO_2–ZnO NP platform was synthesized. The viability of ER positive and TNBCs following exposure to MSNPs-Zn was evaluated and compared to healthy breast epithelial cell and macrophage cell models *in vitro* to define a dose-window for their use. Uptake of the MSNPs-Zn by the TNBCs and the evolution of particle morphology in the intracellular environment were studied using analytical a transmission electron microscope (TEM).

2. Materials and methods

2.1. MSNP synthesis and Zn incorporation

500 mL H_2O, 1 g CTAB and 3 mL NaOH (2 M) were stirred on a hot plate and left to reach 70°C before adding 5 mL tetraethylorthosilicate (TEOS) and, after 1 min, 5 mL ethyl acetate. After 30 s, the stirring was turned off and the solution was left on the hot plate for a further 2 h before centrifugation. The particles were then washed three times in ethanol by cycles of sonication followed by centrifugation [29].

Zinc nitrate was added to the particle suspension on the third washing cycle at molar ratio of Zn: TEOS of 1:1. All particles were then dried overnight in a 60°C oven before calcination at 550°C for 16 h to remove CTAB and nitrates. The cation-containing particles were also washed three times in 1 M NaOH after heating.

2.2. NPs composition analysis

The composition of the MSNPs-Zn was determined using inductively coupled plasma optical emission spectroscopy (ICP-OES, Thermo Scientific ICap 6000 series) following acid digestion of the nanoparticles using the lithium metaborate fusion method. 50 mg of finely ground nanoparticles was mixed with 250 mg of lithium metaborate (Sigma) in a clean dry platinum crucible. The mixture was fused for 40 min at 1,050°C and left to cool. The flux was subsequently dissolved in 2 M nitric acid and transferred to a 100 mL polypropylene volumetric flask before diluting in 2 M nitric acid a further 10 times to a concentration suitable for ICP-OES analysis. The ICP gives the concentration of Si and Zn in mg/L based on which the molar percentage of Zn was calculated using Eq. (1):

$$mol\%\ of\ Zn = \frac{[Zn]\left(\frac{mol}{L}\right)}{[Zn]\left(\frac{mol}{L}\right) + [Si]\left(\frac{mol}{L}\right)} \times 100\% \quad (1)$$

50 mg of nanoparticles was initially dissolved to obtain a concentrated 100 mL stock solution, which was then diluted 10 times for ICP analysis; therefore, the weight percentage of Zn was calculated with Eq. (2) as:

$$\text{wt\% of Zn} = \frac{Conc.\ Zn\left(\frac{mg}{L}\right) \times 10 \times 0.1\ (L)}{50\ mg} \times 100\% \quad (2)$$

2.3. Nanoparticle characterization

Particle size was investigated using dynamic light scattering (DLS, Malvern instrument 2000), and zeta (ζ) potential values were measured in distilled water in three different pH: 3.0, 7.4, and 11.0 using a Zeta sizer (Malvern instrument 2000). Nanoparticles were dispersed in ethanol by sonication (30 s) before being drop cast on a 300 mesh holeycarbon Cu grid (TAAB). Scanning transmission electron microscopy (STEM)-high-angle annular dark field (HAADF)/energy dispersive X-ray spectroscopy (EDX) mapping analyses were performed in a JEOL 2100F scanning/transmission electron microscope (S/TEM) operated at 200 kV, fitted with a X-MaxN Silicon Drift Detector with a detector sizes of 80 mm^2. STEM experiments were performed with a convergence semiangle of 14 mrad and inner and outer HAADF collection angles of 49 and 239 mrad, respectively. The probe diameter was <0.5 nm.

2.4. Cell culture

MDA-MB-231, MCF-7, and MCF-10a cell lines were purchased from ATCC (Manassas, VA, USA). MDA-MB-231 and MCF-7 were maintained in Dulbecco's Modified Eagle Medium (DMEM) and minimal essential media (MEM), respectively. MEM and DMEM media were supplemented with 10% fetal bovine serum (FBS) and

penicillin/streptomycin solution (10,000 units/mL penicillin, 10,000 μg/mL streptomycin). Cells were maintained in a humidified incubator at 37°C and 5% CO_2. MCF-10a cells were grown in DMEM:F-12 supplemented with 20 ng/mL epidermal growth factor (Invitrogen, Life Technologies Ltd, UK), 100 ng/mL cholera toxin (Sigma-Aldrich Ltd, UK), 0.01 mg/mL insulin, 100 ng/mL hydrocortisone, and 5% horse serum. MCF-10a cells were maintained in a humidified incubator at 37°C and 5% CO_2.

To obtain bone marrow macrophages, bone marrow cells were isolated from femur and tibia bones from 6 to 8 week old mice (Balb/c, Female, SKn7204, Harian UK Ltd.) with PBS. Cells were first collected by centrifugation (1,500 rpm, 5 min) and further seeded for 8 days at a concentration of 5×10^5 cells/mL in RPMI cell culture medium (L-Glutamine, Fisher Scientific) containing 10% FBS, 10,000 units/mL penicillin, 10,000 μg/mL streptomycin (Sigma), 0.01% beta-mercaptoethanol (Fisher Scientific), and 0.1 μg/mL macrophage colony-stimulating factor (Peprotech). Non-adherent cells were washed out, and adherent cells were harvested with EDTA and seeded at a concentration of 7.5×10^5 cells/mL for further experiments.

2.5. Viability: cell metabolic activity (WST-1)

The cell metabolic activity following MSNP treatment was determined using Cell Proliferation Reagent WST-1 assay (Roche Applied Biosystems) according to the manufacturer's instructions with modifications. WST-1 assay is a colorimetric assay that can be used to measure cell viability by monitoring mitochondrial metabolic activity. The bioreduction of tetrazolium salt to formazan dye directly correlates to the number of metabolically active cells, therefore viable cells, in the sample. Cells were seeded in a 96-well plate with a density of 15×10^3 cells per well and silica NPs containing Zn (3 replicates per concentration) at NPs concentrations of 25, 50, 100, 150, 200, and 250 μg/mL. After 24 h, media was removed, and the cells were washed once with Hanks' Balanced Salt solution (Sigma). WST-1 reagent was diluted with the medium to 5% (v/v) in the dark, and the plates were then treated with 100 μL of WST-1 5% solution and incubated in a humidified atmosphere at 37°C and 5% CO_2 for 2 h. Spectrophotometric evaluation was performed by measuring the absorbance of the formazan product at 430 nm wavelength. The relative viability (% mitochondrial activity compared to untreated cells) was calculated as mean value ± standard error of the mean (SEM) as a result of at least three independent experiments.

2.6. Cell death

2.6.1. Total DNA content

For total amount of DNA, macrophage cells were seeded at a density of 7.5×10^5 cells/mL in a flat-bottomed 24-well plate and incubated at 37°C and 5% CO_2 for 24 h to allow the cells to form a monolayer. Cells were exposed to the MSNPs at the concentration range 0–250 μg/mL for 24 h. The treated cells were washed 3 times with PBS to remove excess MSNPs. The plates were frozen at −80°C overnight and then thawed at room temperature (RT). 180 μL of molecular water was added in each well, then 20 μL of 100 μg/mL of Hoechst 33258 per well (a final concentration of 10 μg/mL). The fluorescence was measured at excitation wavelength 350 nm and at emission wavelength 460 nm.

2.6.2. Cell apoptosis

The apoptosis TUNEL assay, which detects the fragmented DNA induced by apoptosis by labeling them with a red color fluorescence dye, was also performed.

2.6.3. Data analysis

Data are presented as means ± SEM of independent experiments. Statistical analysis was performed using a one-way analysis of variance (Origin) to assess the statistical significance between the MSNPs and MSNPs-Zn groups. The p-values<0.05 were considered statistically significant.

2.6.4. Cell uptake (TEM)

Cells were seeded in a 6-well plate with a density of 150×10^3 cells per well and incubated with a subtoxic concentration of MSNPs-Zn of 50 μg/mL for 24 h. Cells were rinsed briefly in saline (0.9% NaCl) to remove any non-ingested particles and were then fixed in 2% glutaraldehyde (Sigma) and 2% formaldehyde (Sigma) in 0.1 M sodium cacodylate (Sigma) buffer at pH 7.4 for 1 h at RT. The fixatives were then removed by washing cells with 0.1 M sodium cacodylate buffer for 3 times. Cells were scraped and transferred into 1.5 mL Eppendorf tubes and cell pellets were obtained by centrifugation at 10,000 g for 20 min. Samples were embedded without bulk staining with osmium tetroxide. They were dehydrated in graded ethanol series of 50%, 70%, 95%, and 100% (v/v ethanol to DI H_2O) ethanol for 5 min each, then rinsed three times in acetronitrile (Sigma) for an additional 10 min each, all at RT. After dehydration, samples were progressively infiltrated with an Epon-based resin, created by combining 23.5 g epoxy embedding medium (Sigma), 12.5 g dodecenylsuccinic anhydride (Agar scientific), 14 g methyl acid anhydride (Agar scientific), 0.75 mL benzyl dimethylamine (Agar Scientific). Samples were first resuspended in 25% resin/acetonitrile solution (volume ratio of resin to acetonitrile) and centrifuged for 30 s at 2,000 g. This step was repeated with 50, 75, 100, 100, and 100% resin. Samples were cured at 100°C for 2 h. Thin sections (70 nm) were cut directly into a water bath using an ultramicrotome with a diamond knife with a wedge at an angle of 35°. Sections were immediately collected on bare, 250 mesh TEM grids (Agar Scientific), dried, and kept under vacuum for TEM analysis. Low-resolution TEM imaging was taken by JEM-2100F TEM. HRTEM and STEM-HAADF/EDX analyses were performed in an FEI Titan 80–300 S/TEM operated at 80 kV, fitted with Cs (image) corrector and SiLi EDX spectrometer (EDAX, Leicester UK).

2.6.5. Solid state MAS nuclear magnetic resonance

All ^{29}Si single pulse solid-state MAS nuclear magnetic resonance (NMR) measurements were performed at 7.0 T using a Varian/Chemagnetics InfinityPlus spectrometer operating at a Larmor frequency of 59.6 MHz. These experiments were performed using a Bruker 7 mm HX probe which enabled a MAS frequency of 5 KHz to be implemented. Flip angle calibration was performed on a solid kaolinite sample from which a $\pi/2$ pulse time of 5.5 μs was measured. All measurements were undertaken with a $\pi/4$ tip angle along with a recycle delay between subsequent transients of 240 s. Heteronuclear ^1H decoupling with a nutation frequency of 50 kHz was implemented during data acquisition. All ^{29}Si chemical shifts were reported against the IUPAC recommended primary reference of $Me_4Si_{(l)}$ (1% in $CDCl_3$, δ 0.0 ppm), via a secondary kaolinite$_{(s)}$ reference in which has a known shift of −92.0 ppm [30].

3. Results and discussion

A fabrication method for degradable porous silica NPs platforms with tuneable zinc loading was developed (Fig. 1a). The silica network was synthesized through hydrolysis of TEOS and condensation of the resulting Si–OH groups. The high pH creates nanoparticles. Ordered mesopores were introduced using CTAB as a liquid crystal template while the silica network gelled, producing MSNPs. Zinc nitrate was added into MSNPs in aqueous solution to

allow the formation of Zn^{2+} rich layer on NPs surface. Calcination (550°C, 3 h) promoted diffusion, and incorporation, of zinc ions into the silica matrix and simultaneously burned off the CTAB. The excess of zinc nitrate remaining outside the NPs decomposed into zinc oxide and was removed by a base washing step.

HAADF-STEM imaging (Fig. 1b) and STEM-EDX analysis confirmed the presence of Zn and its homogenous distribution within the MSNPs-Zn (Fig. 1d and e). Excess zinc nitrate was needed to ensure zinc incorporation in the silicate network. Increasing the amount of zinc nitrate in the process increased the mol% of Zn that could be incorporated in the nanoparticles (Fig. 1f). A composition of 78 mol% SiO_2 and 12 mol% ZnO was selected.

The MSNPs-Zn had mean diameters of 54.6 ± 8.9 nm, as measured by TEM (n = 100), and had a hexagonal array of pores with a diameter of ~4 nm in diameter (SI Fig. 1). The hydrodynamic size of MSNPs-Zn was 100.9 ± 9.8 nm, as measured by DLS, with a negative zeta potential of − 18.9 ± 0.5 mV.

In vitro cell culture showed that the MSNPs-Zn NPs were toxic to human breast cancer cells but not to non-tumorigenic epithelial cells within a dose window (Fig. 2). The ER+ and TNBC breast cancer cell lines, MCF-7, and MDA-MB-231 were chosen as representative cell models in viability assays, as they best reflect the two main subtypes of breast cancer; hormone receptor positive (ER +/PR +) and hormone receptor negative HER2 negative (TNBC) tumors, respectively. Non-tumorigenic human breast epithelial cell line MCF-10a are often used as a normal cell model [31].

The effect of the MSNPS-Zn and MSNPs on cell viability was first investigated using the WST-1 assay, which measures the mitochondrial metabolic activity of the cells. At concentrations of MSNPs-Zn between 75 and 250 μg/mL, the MDA-MB-231 and the MCF-7 breast cancer cells showed a significant dose-dependent reduction in mitochondrial activity, suggesting that the viability of the cells reduced ($p<0.001$) (Fig. 2a), compared with non-treated controls after 24 h exposure. There was no significant reduction in viability of the non-tumorigenic MCF-10a cells within a dose window of 75–125 μg/mL (boxed region). For example, at 125 μg/mL mitochondrial activity of the MCF-7 and MBA-MD-231 cells was almost zero, whereas the MCF-10a and *murine bone marrow–derived macrophage* (BMM) cells both showed mitochondrial activity above that of the controls. The MDA-MB-231 cells showed a higher sensitivity to MSNPs-Zn than the MCF-7 cells. There was a significant difference in the mitochondrial activity between the MCF-7 and the MDA-MB-231 cells after the exposure to MSNPs-Zn at 75 ($p<0.05$) μg/mL and 100 ($p<0.01$) μg/mL, respectively. The IC_{50} (the half maximal inhibitory concentration, analyzed by Origin, OriginLab) of MSNPs-Zn was 78 and 86 μg/mL for the MCF-7 and MDA-MB-231, respectively. MCF-10a cells showed no reduction in mitochondrial reduction following exposure to concentrations of ≤125 μg/mL of the MSNPs-Zn. The IC_{50} value of MSNPs-Zn for the MCF-10a cells was 141 μg/mL, which was much higher than the MCF-7 and MDA-MB-231 cells. None of the cells experienced a reduction in their mitochondrial activity after the exposure to MSNPs without Zn (Fig. 2b); only the MDA-MB-231 showed a

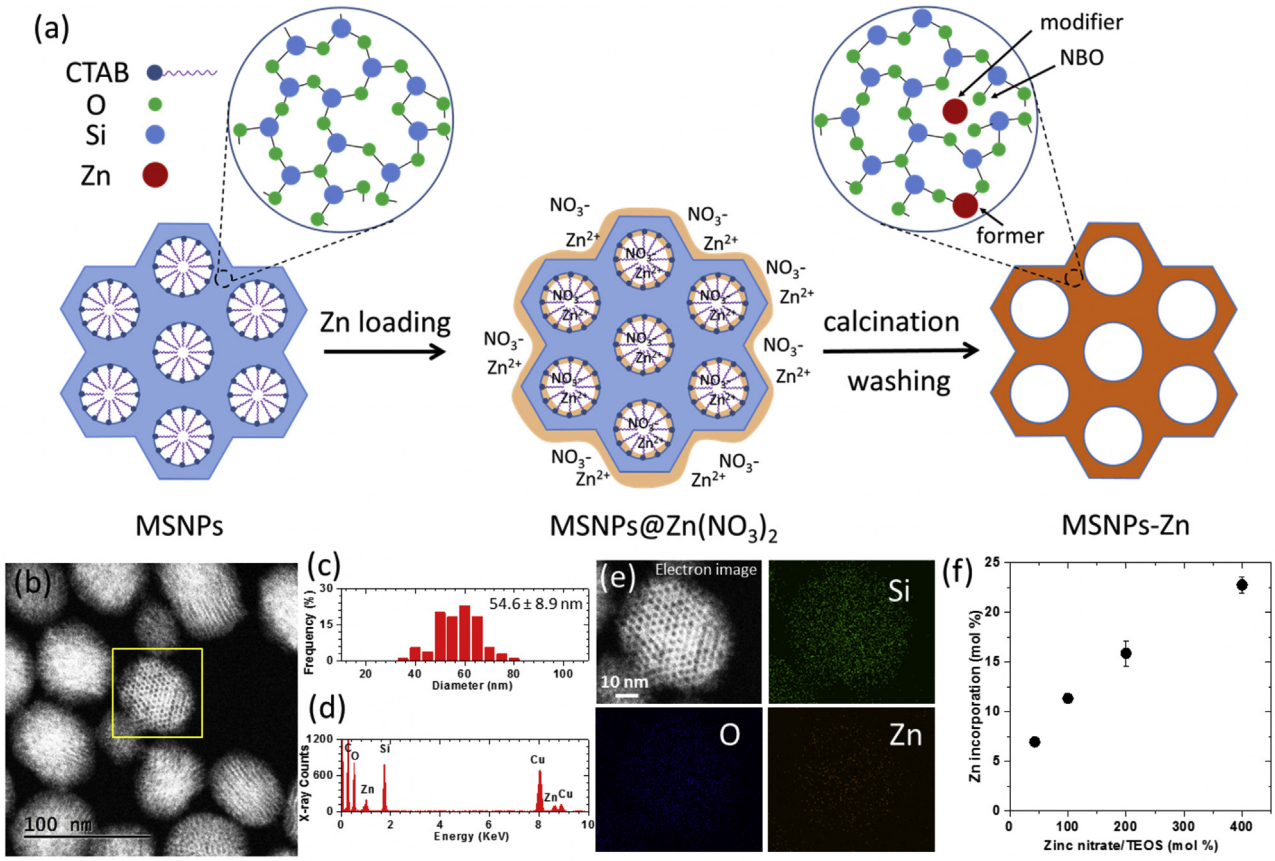

Fig. 1. MSNP-Zn NP fabrication and characterization: (a) schematic illustrating the procedure used to fabricate the MSNPs-Zn; (b) A high-angle annular dark field-scanning transmission electron microscopy image of the MSNPs-Zn; (c) MSNP-Zn NP diameter distribution (n = 100); (d) EDX spectrum collected from the boxed area in (b) showing Zn presence; (e) corresponding STEM-EDX elemental maps; (f) linear relationship between the initial zinc nitrate to TEOS ratio and the final zinc incorporation into the MSNPs-Zn. The amount of zinc loading into the MSNPs-Zn was measured by ICP-OES (n = 3). ICP-OES, inductively coupled plasma optical emission spectroscopy. MSNPs-Zn, zinc-containing mesoporous silica nanoparticles; STEM, scanning transmission electron microscopy.

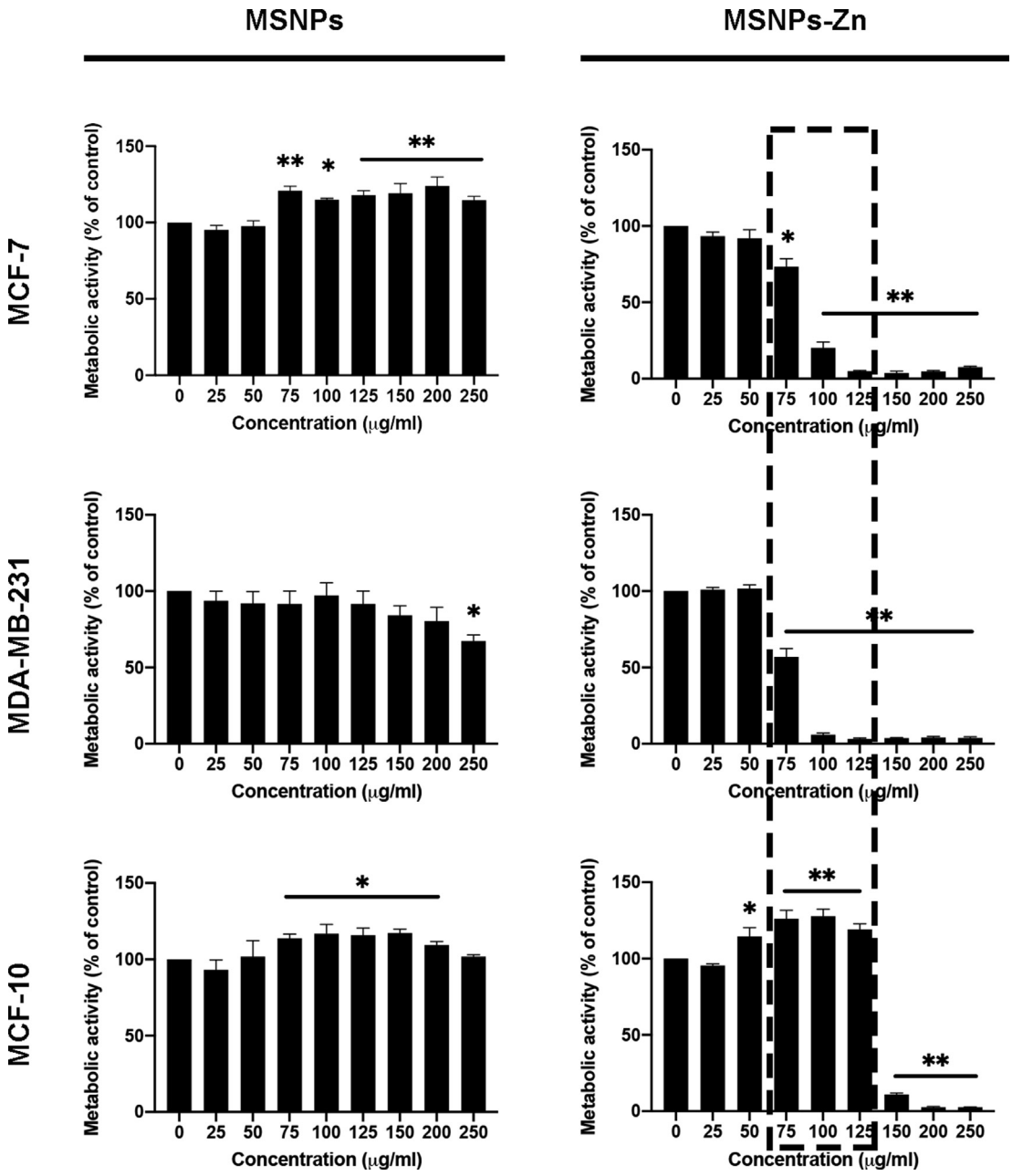

Fig. 2. Metabolic activity (WST-1 viability assay) of breast cancer cell lines MCF-7 and MDA-MB-231 following treatment with MSNPs and MSNPs-Zn for 24 h. MSNPs-Zn significantly reduced the viability of MCF-7 and MBA-MD-231 breast cancer cells at a dose of 75 μg/mL or above, with no significant reduction in viability of the non-tumorigenic MCF-10a cells within a dose window of 75–125 μg/mL (boxed region). Error bars are mean ± SD (n = 3). The *p*-values of $p<0.05$ and $p<0.001$ are considered significant and are denoted with * and ** symbol, respectively. MSNPs-Zn, zinc-containing mesoporous silica nanoparticles.

reduction in mitochondrial activity of ~33% with a significance of $p<0.01$ compared with the non-treated control cells.

The mononuclear phagocyte system, which consists of resident macrophages predominantly in the spleen, lymph nodes, and liver, could pose a major barrier for nanoparticles to reach the disease sites because of the non-specific uptake of nanoparticles and clearance by the phagocytic cells. Monocyte-macrophage precursors are initially generated in the bone marrow, from there they enter the peripheral blood stream and move into the peripheral tissues, where they undergo specific differentiation to become resident macrophage cells (e.g. Kupffer cells in the liver, alveolar macrophage cells in the lung, splenic macrophage cells in the spleen, etc.), depending on the local tissue environment [32]. For this reason, BMM cells were used to evaluate uptake of MSNPs-Zn by macrophages and their effect on cell viability (Fig. 3).

The BMM cells experienced an increase in mitochondrial activity after 24 h of exposure to MSNPs-Zn in a concentration range between 25 and 250 μg/mL (Fig. 3). BMM cells treated with the highest concentration of MSNPs-Zn (250 μg/mL) showed <15% reduction of DNA ($p<0.05$) after 24 h. Reduction of DNA and consequently cell number could be ascribed to apoptosis. To determine if the reduction of BMM cell number was mediated by the MSNPs-Zn, the TUNEL assay was used. The MSNPs-Zn did not induce significant apoptotic cell death of BMMs at 25 and 200 μg/mL after 24 h, indicated by the absence of a red fluorescence signal in the TUNEL assay (Fig. 3), even though particles were internalized

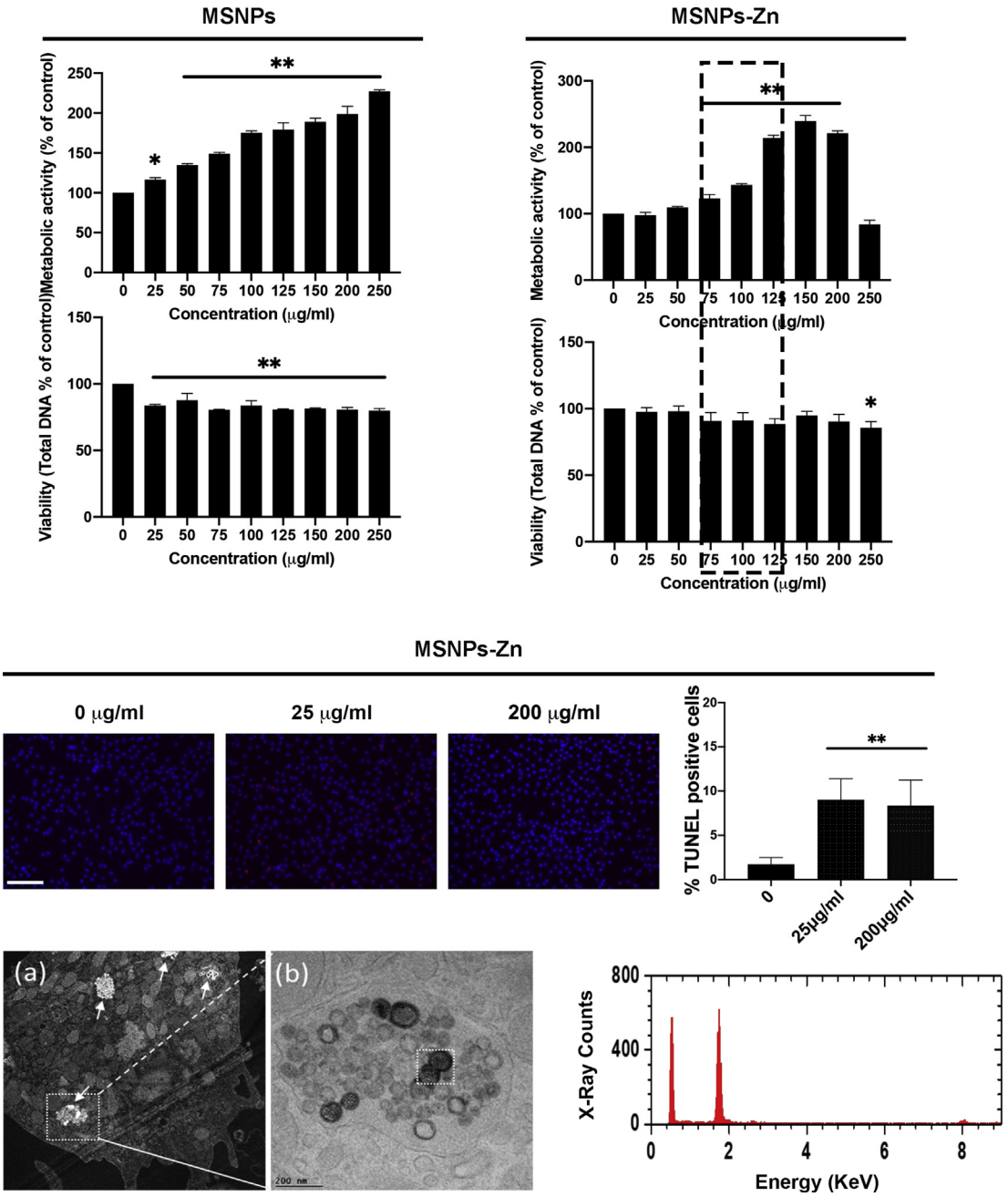

Fig. 3. Effect of MSNPs and MSNPs-Zn on BMMs exposed for 24 h. Top panel: Murine bone marrow macrophage cell (BMM) control and BMMs treated with MSNPs-Zn at concentrations of 25 μg/mL and 200 μg/mL for 24 h. There was no significant reduction in viability of BMM within the therapeutic dose window of 75–125 μg/mL (boxed), as measured by WST-1 metabolic activity assay, including when normalized to total DNA (Hoechst™ 33258 assay), error bars are mean ± SD (n = 3). Middle panel: The TUNEL assay was used to assess apoptotic cell death at the lowest (25 μg/mL) and highest (200 μg/mL) MSNPs-Zn doses. Absence of a red fluorescence signal (left) indicates that the MSNPs-Zn did not induce significant apoptotic cell death on the BMM cells at 25 and 200 μg/mL after 24 h. Quantification of TUNEL-positive cells agreed (right). Bottom panel: HAADF-STEM demonstrated the uptake of MSNPs-Zn inside BMMs after 24 h exposure at a concentration of 200 μg/mL (left); (a) Location of MSNPs-Zn is marked by arrows; (b) a higher resolution BF-TEM image of the boxed area in the HAADF-STEM image shows the morphology of MSNPs-Zn after 24 h incubation with BMM cells, particles were found inside vesicle-like structures which are likely to be phagosomes (arrows). The MSNPs-Zn had a hollow structure and STEM-EDX spectrum (right) collected from the boxed area showed Zn was absent from the particles indicating complete release of Zn into the BMM cells after 24 h. Scale bar, 1 mm n = 3. The data are expressed as mean ± SEM. *p<0.05, **p<0.001. MSNPs-Zn, zinc-containing mesoporous silica nanoparticles; HAADF-STEM, high-angle annular dark field–scanning transmission electron microscopy.

by the BMMs. STEM images showed the particles inside vesicles within the BMMs and EDX revealed that the particles no longer contained zinc.

Taken together, these results suggest a promising therapeutic dose window of 75–125 μg/mL, within which MSNPs-Zn demonstrate that can selectively be toxic to the breast cancer cells without affecting healthy epithelial of BMM cell viability. These findings support previous work on soluble ZnO nanoparticles that showed Zn^{2+} ions caused cell death for MCF-7 and MDA-MB-231 TNBC breast cancer epithelial cells [27], where cell death can be attributed to generation of reactive oxygen species, resulting in damage to the plasma membrane [25]. TNBCs are often resistant to classic treatments, so the MSNPs-Zn could act to intensify conventional chemotherapeutics.

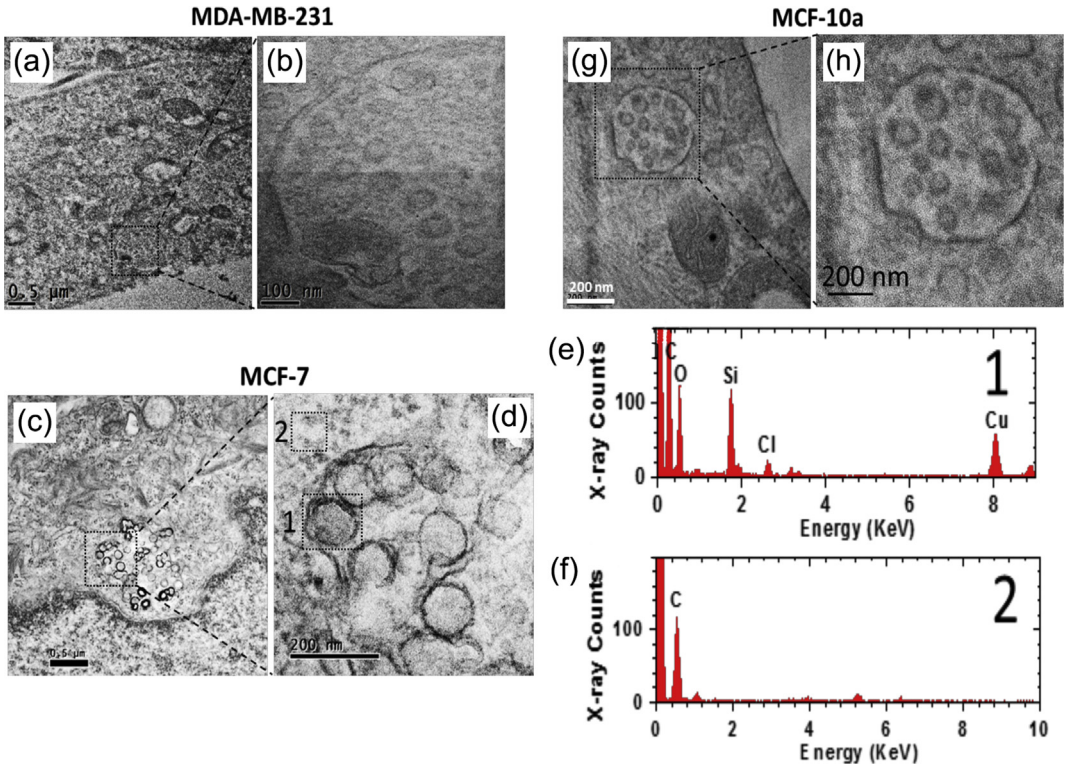

Fig. 4. (a–d) TEM images showing MSNPs-Zn internalized by the different cell types and the particles were degraded with 'ghost-like' hollow structures: (a,b) MSNPs-Zn inside MDA-MB-231 cells; (c, d) MSNPs-Zn within MCF-7 cells; (e, f) EDX spectra collected from the boxed areas (1, 2) respectively in (d); (g, h) TEM images of MSNPs-Zn degraded inside non-cancerous MC7-10a cells. MSNPs-Zn, zinc-containing mesoporous silica nanoparticles; TEM, transmission electron microscope.

TEM of sections of the cells revealed that the MSNPs-Zn released Zn and degraded in the intracellular environment of the MDA-MB-231 cells after 24 h exposure. MSNPs had altered morphology inside lysosome/endosome-like vesicles after 24 h incubation with MDA-MB-231 cells at a concentration of 50 μg/mL (Fig. 4a and b), with ghost-like, hollow structures observed inside the cancer cells. The structures had a diameter of 100 nm, which was larger than the size of the original particles measured by TEM, indicating that the particles degraded and a silicate, or mineral, shell have formed. The particles also seemed to have degraded more rapidly inside cancer cells and epithelial cells (Fig. 4) than in BMMs (Fig. 3) or in acellular conditions (Figs. 5 and 6). Formation of hollow silica structures has been observed previously for mesoporous silica NPs in ultrapure water [33], which was attributed to those particular particles having a lower degree of silica condensation in the inner section than the outer layer, according to NMR characterization of the nanoparticles [33]. Preferential dissolution of inner section in water was thought to have led to hollow structure formation. Here, our particles were calcined. However, proteins may bind to the MSNPs-Zn surfaces, forming a corona, in a similar manner as observed previously *in vitro* in the presence of serum, which increased the stability of the surface of

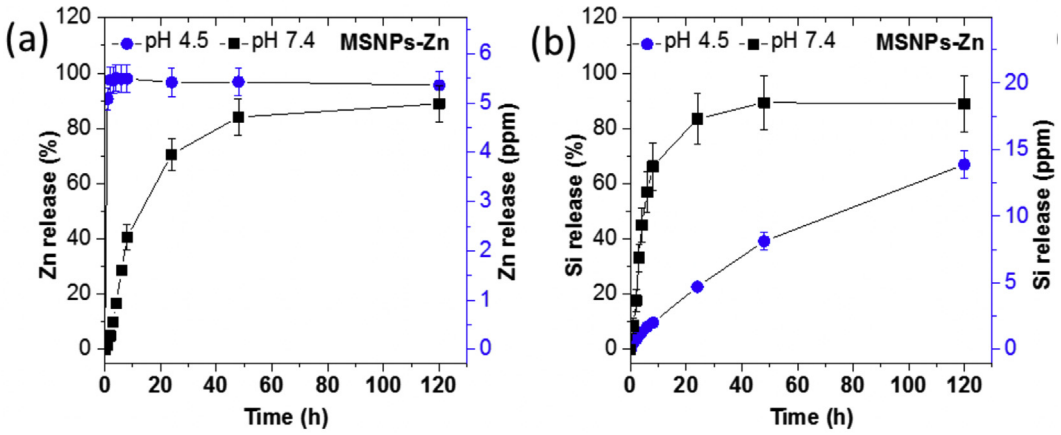

Fig. 5. Dissolution profiles of NaAC/HAC buffer (pH 4.5) and Tris/HCl buffer (pH 7.4), from ICP-OES analysis, following immersion of MSNPs-Zn: (a) Zn release profiles from the MSNPs-Zn; (b) Si release profiles from the MSNPs-Zn. Metal ion release and NP degradation was pH dependent. The rate of Zn release was higher in lower pH conditions, while Si release, indicative of degradation of silica network, was faster in a higher pH environment. MSNPs-Zn, zinc-containing mesoporous silica nanoparticles; ICP-OES, inductively coupled plasma optical emission spectroscopy.

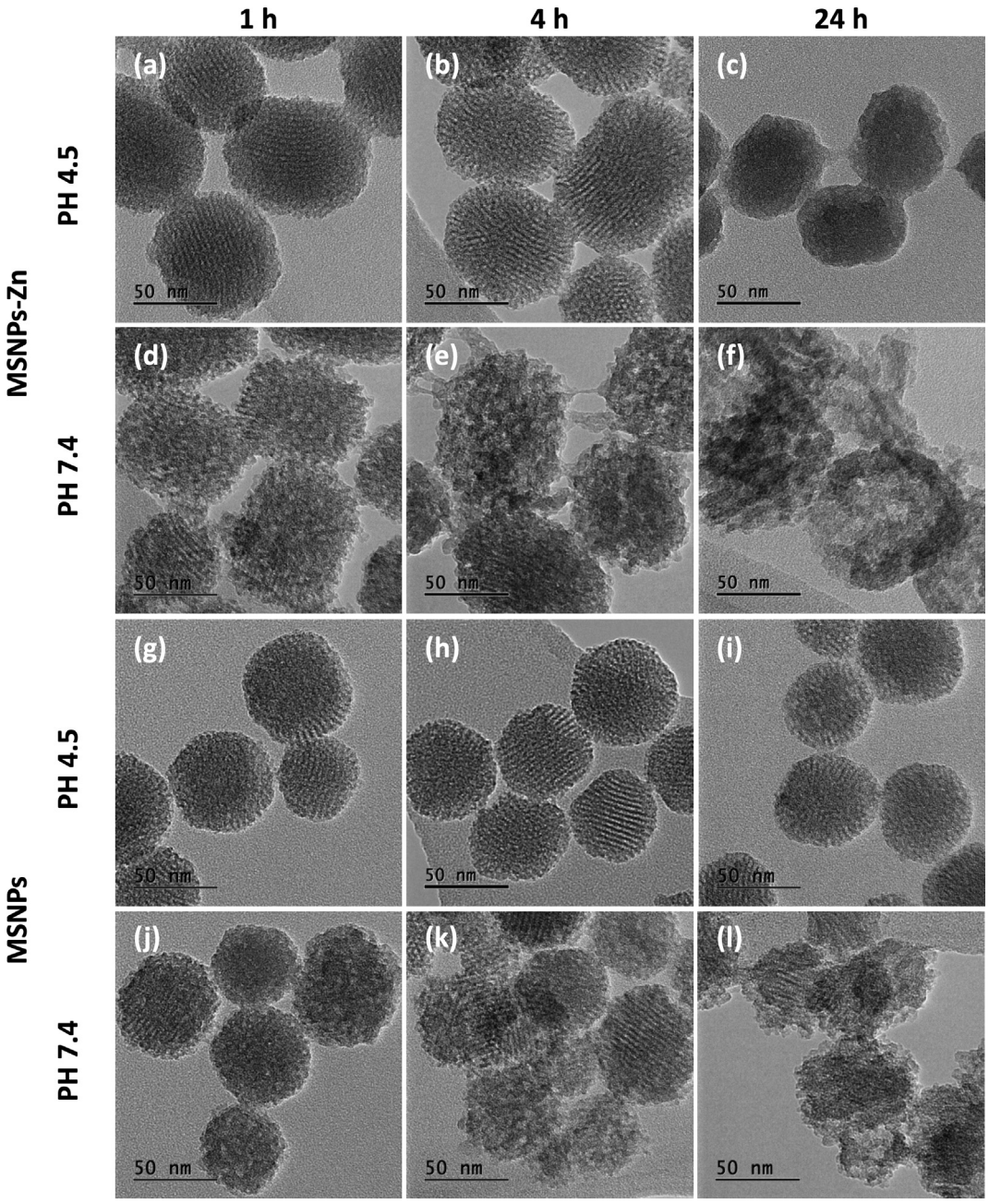

Fig. 6. TEM images showing the evolution in the morphology of MSNPs ± Zn during incubation at pH 4.5 or pH 7.4 for 1, 4, and 24 h, respectively: (a–f) MSNPs-Zn; (g–l) MSNP controls. The NPs were extracted and washed with DI water for imaging. MSNPs-Zn, zinc-containing mesoporous silica nanoparticles; TEM, transmission electron microscope.

the MSNPs [34]. Similar 'ghost' structures were previously observed on the surface of ZnO nanowires inside human monocyte derived macrophage cells [35].

Similar structural changes to the MSNPs-Zn were found within the MCF-7 (Fig. 4c and d) and MCF-10a (Fig. 4g and h) cells. The elemental composition of the structures (Fig. 4d, area 1) was further characterized by STEM-EDX, which showed that the ghost-like particles were composed of silicon and oxygen and devoid of any zinc (Fig. 4e). The lack of a calcium or phosphorous peak indicates that the shell was not mineral. The carbon, copper, and part of the oxygen signals arises from the polymer used to embed the cells and the copper TEM grid. Fig. 3f shows an area without particles (area 2), which was collected as a control, and EDX confirmed it was devoid of any silicon.

MSNPs without Zn degraded to a lesser extent inside the MCF-10a cells (SI Fig. 2). Although some of the MSNPs appeared to have degraded from the inside of the particles, many of MSNPs still maintained their mesoporous characteristics. These analyses demonstrate that the incorporation of zinc ions increased the dissolution rate of the nanoparticles inside the cells, enabling control of biodegradation rate of the NPs. An explanation for the reduced stability is that a fraction of the zinc ions play a role as a network modifier (or intermediate) inside the silica network, creating non-bridging oxygens by breaking down the silicon-

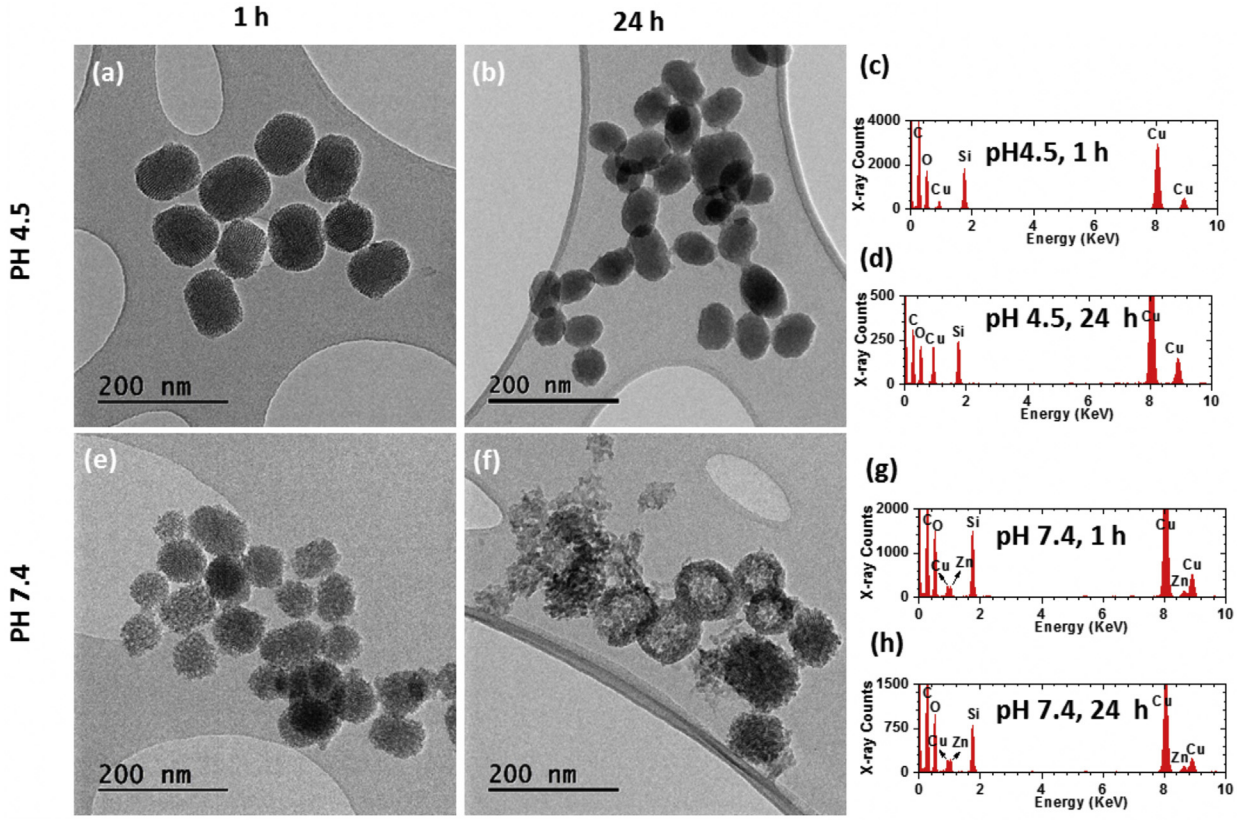

Fig. 7. TEM analysis of MSNPs-Zn incubated in pH 4.5 and pH 7.4 for 1 h and 24 h. (a-b, e-f): BF-TEM images of the areas from which TEM-EDX patterns were collected (c-d, e-f). MSNPs-Zn, zinc-containing mesoporous silica nanoparticles; TEM, transmission electron microscope.

oxygen covalent bonds, which leads to a biodegradable silicate network [36].

The BMM cells remained healthy even after incubation with MSNPs-Zn concentrations of 200 μg/mL for 24 h (Fig. 3). The MSNPs-Zn were found inside vesicle-like structures, which were likely to be phagosomes or phagolysosomes. A similar hollow morphology for the MSNPs-Zn was observed (Fig. 3b), and an absence of Zn detected in remaining particulate structures indicates complete release of the Zn in the BMM cells after 24 h.

We further investigated the mechanism of structural degradation of MSNPs-Zn and MSNPs as a function of time and pH using ICP and high resolution TEM. Sodium acetate/acetic acid (NaAC/HAC) buffer (pH 4.5) and Tris/HCl buffer (pH 7.4) were employed to study the pH influence on the dissolution and degradation of MSNPs-Zn and MSNPs. Buffer solutions containing phosphate, such as artificial lysosomal fluid (ALF), simulated body fluid (SBF) and cell culture media, are not suitable to use to study the effect of pH of ion release from the MSNPs because the zinc forms highly insoluble $Zn_3(PO_4)_2$ ($K_{sp} = 9.0 \times 10^{-33}$) with phosphate and the formation of silica rich layer on the NP surface through the condensation of dissolved Si—OH groups can trigger the formation of $CaO—P_2O_5$ layer [37].

The release of Zn was much more rapid at pH 4.5 and silica release was more rapid at pH 7.4 (Fig. 5), indicating zinc was preferentially released at pH conditions similar to those in the intracellular vesicles they were imaged in (Figs. 3 and 4). The rate of silica release and breakdown of the silicate network was more rapid at neutral pH, with ~75% of the silica lost from the particles at 8 h, compared with only ~10% at pH 4.5. The much more rapid zinc release at pH 4.5 (90% lost in 2 h) and the low sustained release at pH 7.4 (less than 5% of Zn had dissolved from the leached out from MSNPs-Zn at pH 7.4 after 2 h) is encouraging as it shows some selectivity in terms of Zn^{2+} ion release; it will be faster at a low pH tumor environment and rapid in a lysosome, but slow in blood plasma.

TEM showed that the change in morphology of the MSNPs-Zn was more significant at pH 7.4 than at pH 4.5. No substantial change in the morphology MSNPs-Zn was observed after 1 and 4 h incubation at pH 4.5 (Fig. 6a and b). The nanopores were clearly visible within the particles. After 24 h, some degradation of the outer shell of the MSNPs-Zn was seen, and the particles lost their mesoporous appearance. At pH 7.4, after 1, 4, and 24 h, the pore size and the surface roughness of NPs surface increased (Fig. 6d and e). After 24 h at pH 7.4, the MSNPs-Zn started to lose relative density in their centers (Fig. 6f). Some degradation of the outer surface of the MSNPs-Zn was also observed at pH 7.4; however, this was less marked, suggesting that degradation of MSNPs-Zn proceeded preferentially from the inside of the spheres.

In general, the MSNPs were less susceptible to degradation than the MSNPs-Zn. At pH 4.5, the MSNPs remained as spheres of similar size and had not lost their porous structure at 24 h (Fig. 6g—i). And at pH 7.4, an increase in surface roughness were observed for the MSNPs after 1 h incubation (Fig. 6j). After 4 and 24 h, the change in the MSNPs morphology became more significant; however, some of the MSNPs without Zn still had an unaltered mesoporous structure suggesting a slower degradation rate of the Zn containing MSNPs (Fig. 6k and l compared to Fig. 6d and e).

STEM-EDX analysis of MSNPs-Zn shows that all of the zinc had been released after 1 h at pH 4.5 but they still contained Zn after 24 h immersion in buffer at pH 7.4 (Fig. 7), supporting the

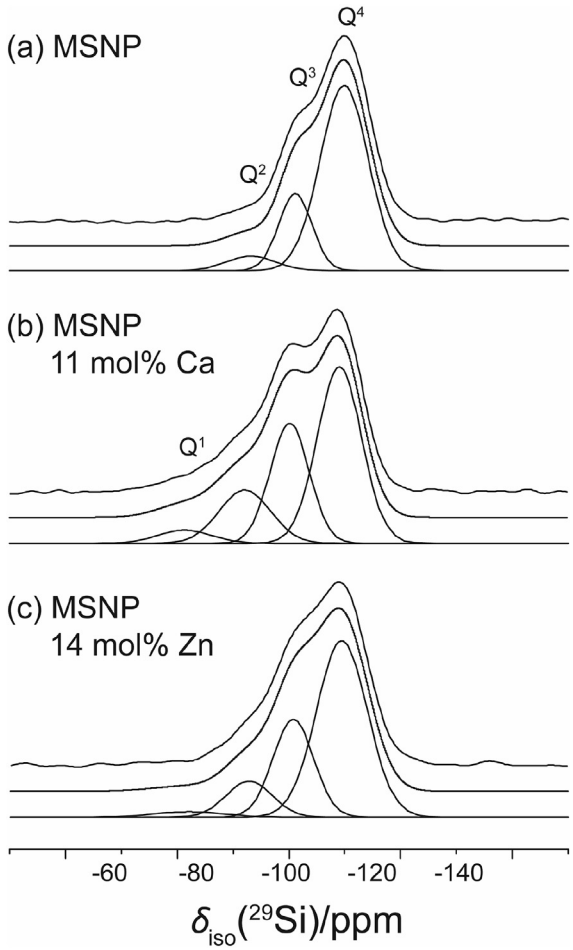

Fig. 8. Single ^{29}Si solid-state NMR data for mesoporous silica (MSNP), mesoporous particles of the 89 mol% SiO_2, 11 mol% CaO (MSNP-Ca) and 86 mol% SiO_2, 14 mol% ZnO (MSNP-Zn). Q^n refers to Si with n bridging oxygen bonds and 4-n non-bridging oxygen bonds. MSNP, mesoporous silica nanoparticle; NMR, nuclear magnetic resonance.

respectively) reduced in comparison to that of the zinc-free silica nanoparticles (MSNP). The relative Q^4 content (i.e. silicon connected the maximum of four bridging oxygen bonds) was 73% for MSNP, which reduced to 49% and 60% for MSNP-Ca and MSNPs-Zn, respectively. Of particular note is that MSNPs-Zn system (composition 86 mol% SiO_2, 14 mol% ZnO) exhibited greater residual connectivity through the presence of more observable Q^4 species than the corresponding MSNP-Ca system (composition 89 mol% SiO_2, 11% CaO), for a greater divalent cation incorporation. This suggests that the zinc participates in both network forming and network modifying roles within the glass and therefore an important role in control of the degradation rate, particularly in regard to the changes in degradation rate with pH (SI Fig. 5).

The zinc speciation defining network modification (ionic $-SiO^- \cdot Zn^{2+}$ moieties) and network formation (covalent -Si-O-Zn-O-Si- linkages) induce very different chemical responses under acidic and physiological pH (7.4) conditions. In acidic conditions (pH ~4.5), zinc is released by efficient cation exchange with H^+ and complete hydrolysis extends to all ionic and covalently zinc species represented by Eqs. (1) and (2) below:

$$2(\text{-Si-O}^-)\cdot Zn^{2+} + 2H^+ \rightarrow 2(\text{-Si-OH}) + Zn^{2+} \quad (3)$$

$$-Si-O-Zn-O-Si- + 2H^+ \rightarrow 2(-Si-OH) + Zn^{2+} \quad (4)$$

This explains the rapid zinc release in acidic environments (Fig. 5a), where aggressive hydrolytic zinc release is facilitated by both cation exchange with H^+ and cleavage of the Zn—O covalent bond. However, under milder hydrolysis conditions, at pH 7.4, a two-stage zinc release process was observed (Fig. 5a). Initially, a relatively fast zinc release was measured (i.e. ~40% zinc released by 8 h) because of the replacement of network modifier Zn^{2+} by H^+ cation exchange (Eq. (3)), but the release of the covalently bonded zinc release was a slower process, which relies on the cleavage of the Zn—O bonds (Eq. (4)) and subsequent break down of the silica network. After the rapid initial release of Zn, the slower zinc dissolution rate was characterized by a more gradual release up to 70% after 48 h (Fig. 5b).

Table 1
Summary of single pulse^{29}Si solid-state NMR data for mesoporous silica (MSNP) and mesoporous particles of the 89 mol% SiO_2, 11 mol% CaO (MSNP-Ca) and 86 mol% SiO_2, 14 mol% ZnO (MSNPs-Zn). Q^n refers to Si with n bridging oxygen bonds and 4-n non-bridging oxygen bonds.

Sample	Q^1		Q^2		Q^3		Q^4	
	δ_{Iso} [ppm]	I [%]	δ_{Iso} [ppm]	I [%]	δ_{Iso} [ppm]	I [%]	δ_{Iso} [ppm]	I [%]
MSNP	–	–	−93.3 ± 0.2	5.7 ± 0.3	−101.2 ± 0.1	21.0 ± 0.3	−110.0 ± 0.1	73.3 ± 0.1
MSNPs-Ca	−81.9 ± 0.3	4.4 ± 1.2	−92.8 ± 0.1	17.2 ± 1.2	−101.0 ± 0.9	29.3 ± 0.4	−110.0 ± 0.9	49.1 ± 0.3
MSNPs-Zn	−82.0 ± 1.0	2.5 ± 0.3	−92.8 ± 0.2	11.0 ± 0.3	−100.8 ± 0.1	26.5 ± 0.2	−109.5 ± 0.2	60.0 ± 0.1

NMR, nuclear magnetic resonance; MSNP, mesoporous silica nanoparticle; MSNPs-Zn, zinc-containing mesoporous silica nanoparticles.

hypothesis of preferential/selective zinc release in the acidic intracellular environment and slower zinc release from the MSNPs-Zn in the extracellular environment. HAADF-STEM images and EDX mapping of MSNPs-Zn incubated in pH 7.4 for 24 h confirmed Zn remained in MSNPs-Zn after 24 h incubation in pH 7.4 (SI Fig. 3) and the distribution of Zn was approximately homogeneous. This pH dependent degradation profile could be important for clinical translation of this material, as it will reduce the persistence of particles that reach systemic sites in the body.

Degradation behavior of the nanoparticles is dependent on how the Zn disrupts the silica network so the role of the Zn in the silica network was investigated by solid state NMR. The ^{29}Si MAS NMR data (Fig. 8 and Table 1) demonstrate that the silicate connectivity for Ca- and Zn-incorporated systems (MSNP-Ca and MSNPs-Zn,

4. Conclusions

Monodispersed zinc containing biodegradable mesoporous silica nanoparticle platforms (MSNPs-Zn) for therapeutic cation delivery biodegraded within cells after internalization. MSNPs-Zn were toxic for MDA-MB-231 TNBCs and MCF-7 (ER +) breast cancer cells and in a dose window of 75 and 250 μg/mL, the particles only killed the cancer cells, not the healthy equivalent model cells. The results also demonstrate, for the first time, that the MSNPs-Zn are internalized by both types of breast cancer cells. The MSNPs-Zn showed pH-stimulated cation release. The zinc release from the MSNPs-Zn was much faster in an acidic than in a neutral environment, suggesting that the toxicity of the Zn^{2+} ions to the cancer cells could be attributed to an intracellular effect. Incubation of the

MSNP-Zn at an acidic pH representative of phagosome/phagolysosome pH or a tumor environment triggered rapid zinc ion release and created hollow silica nanoparticles. The MSNP-Zn formed hollow structures inside the cells, which probably commenced in the neutral extracellular environment. At neutral pH, more uniform degradation of the particles was observed. Future work will focus on developing this versatile theranostic platform for combined treatment and imaging of breast cancer cells.

Declaration of competing interest

The authors declare that they have no known competing financial interests or personal relationships that could have appeared to influence the work reported in this paper.

Acknowledgments

The authors acknowledge the EPSRC (EP/M004414/1 and EP/I004734/1) and the Department of Materials (Imperial College London) for funding. J.V.H. also thanks the EPSRC and the University of Warwick for partial funding of the solid-state NMR infrastructure at Warwick and acknowledges additional support for this infrastructure obtained through Birmingham Science City: Innovative Uses for Advanced Materials in the Modern World (West Midlands Center for Advanced Materials Projects 1 and 2), with support from Advantage West Midlands (AWM) and partial funding by the European Regional Development Fund (ERDF). A.E.P. acknowledges an Elsie Widdowson Fellowship for her salary support. Raw data are available on request from rdm-enquiries@imperial.ac.uk.

Appendix A. Supplementary data

Supplementary data to this article can be found online at https://doi.org/10.1016/j.mtadv.2020.100066.

References

[1] B. Sirohi, et al., Ann. Oncol. 19 (11) (2008) 1847.
[2] Slowing II, et al., Adv. Drug Deliv. Rev. 60 (11) (2008) 1278.
[3] Y. Wang, et al., Nanomedicine 11 (2) (2015) 313.
[4] F. Tang, et al., Adv. Mater. 24 (12) (2012) 1504.
[5] M. Colilla, et al., Biomater. Sci. 1 (2) (2013) 114.
[6] K.S. Butler, et al., Small 12 (16) (2016) 2173.
[7] C.E. Ashley, et al., Nat. Mater. 10 (5) (2011) 389.
[8] P.N. Durfee, et al., ACS Nano 10 (9) (2016) 8325.
[9] S. Wilhelm, et al., Nat. Rev. Mater. 1 (5) (2016) 12.
[10] J.R. Jones, Acta Biomater. 9 (1) (2013) 4457.
[11] G. Kaur, et al., J. Biomed. Mater. Res. 102 (1) (2014) 254.
[12] L.L. Hench, J. Mater. Sci. Mater. Med. 17 (11) (2006) 967.
[13] J.R. Jones, et al., Int. J. Appl. Glass Sci. 7 (4) (2016) 423.
[14] K.K. Mitchell, et al., J. Mater. Chem. B Mater. Biol. Med. 2 (45) (2014) 8017.
[15] K.K. Pohaku Mitchell, et al., J. Am. Chem. Soc. 134 (34) (2012) 13997.
[16] A. Liberman, et al., Biomaterials 33 (20) (2012) 5124.
[17] L. Yu, et al., J. Am. Chem. Soc. 138 (31) (2016) 9881.
[18] C. Dai, et al., Biomaterials 32 (33) (2011) 8506.
[19] S. Labbaf, et al., Biomaterials 32 (4) (2011) 1010.
[20] O. Tsigkou, et al., Adv. Healthcare Mater. 3 (1) (2014) 115.
[21] S.L. Greasley, et al., J. Colloid Interface Sci. 469 (2016) 213.
[22] K. Zheng, A.R. Boccaccini, Adv. Colloid Interface Sci. 249 (2017) 363.
[23] Q.J. He, et al., Microporous Mesoporous Mater. 131 (1–3) (2010) 314.
[24] Y. Shi, et al., Langmuir 34 (1) (2018) 406.
[25] A. Sasidharan, et al., Nanoscale 3 (9) (2011) 3657.
[26] C. Hanley, et al., Nanotechnology 19 (29) (2008) 295103.
[27] B.A. Othman, et al., Adv. Healthcare Mater. 5 (11) (2016) 1310.
[28] Z. Nescakova, et al., Bioact. Mater. 4 (2019) 312.
[29] B.S. Chang, et al., Chem. Mater. 25 (4) (2013) 574.
[30] R.K. Harris, et al., Magn. Reson. Chem. 40 (7) (2002) 489.
[31] Y. Qu, et al., PloS One 10 (7) (2015) 16.
[32] P.J. Murray, T.A. Wynn, Nat. Rev. Immunol. 11 (11) (2011) 723.
[33] X.P. Wang, et al., Small 12 (26) (2016) 3510.
[34] A.M. Clemments, et al., ACS Appl. Mater. Interfaces 7 (39) (2015) 21682.
[35] K.H. Muller, et al., ACS Nano 4 (11) (2010) 6767.
[36] D.S. Brauer, Angew. Chem. Int. Ed. 54 (14) (2015) 4160.
[37] L. Bingel, et al., Mater. Lett. 143 (2015) 279.